Finite Element Based Method to Predict Gas Permeability in Cross-ply Laminates

JIANLONG XU* AND BHAVANI V. SANKAR
Department of Mechanical and Aerospace Engineering, University of Florida
P.O. Box 116250, Gainesville, Florida, 32611-6250, USA

SATISH BAPANAPALLI
Battelle - Pacific Northwest National Laboratory, Richland, WA 99354, USA

ABSTRACT: A finite-element based method is developed to predict gas permeability in cross-ply laminates. Based on Poiseuille's Law and Darcy's Law, the gas permeability is presented in terms of crack densities, microcrack opening displacements and an experimentally determined constant. The crack densities in each ply are predicted using finite element analysis based on energy concept of micro-fracture mechanics. The microcrack opening displacement of the representative volume element in cross-ply laminate is computed using three-dimensional finite element analysis. The normalized gas permeability in three laminates with different lay-ups are predicted and compared using the current model. Finally, a permeability-related material constant is quantified using the experimental results available in the literature.

1 **KEY WORDS:** ▮▮▮.

INTRODUCTION

COST REDUCTION OF sending payload to space is a major issue in a future single-stage reusable launch vehicle (RLV). Various gas storage tanks constitute about 50% of the dry weight of space vehicles. Hence, reducing their weights can significantly reduce the launch cost. Graphite/epoxy composite laminate had been identified as a main candidate for the liquid fuel tank due to its high strength/weight ratio. Replacing conventional metallic tank with the same strength composite tank could save 30% in weight [1]. However, gas leakage through composite laminates has caused a set back to the application of graphite/epoxy composite laminates to the liquid hydrogen storage tanks. The microcracks and delaminations introduced by mechanical/thermal and cyclic loading are believed to be the main reason for gas permeability, since the permeation due to

2 *Author to whom correspondence should be addressed. E-mail: xujl@ufl.edu

0021-9983/08/00 0001–16 $10.00/0 DOI: 10.1177/0021998307088610

Los Angeles, London, New Delhi and Singapore

diffusion is negligibly small. Understanding this mechanism is very essential for proper selection of materials, lay-up, and design of composite cryogenic propellant tanks.

Many researchers have experimentally investigated gas permeability in composite laminates since the failure of the liquid hydrogen tank in X-33 [2–9]. Different lay-ups are tested in experiments such as cross-ply [2–5, 8] and multi-directional ply composites [6–8], and textile composites [9]. Even though hydrogen is the working gas in the propellant tank, due to safety considerations, most researchers use helium gas instead in their experiments [2–5, 8, 9]. The specimens were tested under different conditions: bi-axial loading [2–5], uniaxial loading after thermal cycling [6, 7], or thermal cycling only [8, 9]. It had been found that the permeability is largely dependent on the damage status (crack density), applied loads, lay-ups, and test temperature.

Meanwhile, researchers are seeking some analytical and/or numerical models to predict gas permeability since experimental investigation is usually expensive. These models can be roughly divided into two groups: one is based on Darcy's law for porous media [2–5, 13–15] and the other one is based on fluid mechanics for incompressible Newtonian fluid [6, 10–12]. In the first model, the overall permeability of composite laminate is derived in terms of crack density, crack intersection area, and a material constant that can be determined from experiments [16]. In the second model, a damage network due to microcracking and delamination in composite laminates has been set up and steady gas flow through the network has been simulated using a computational fluid dynamics program (FLUENT) to find the conductance. For both models, the key point is to find the crack densities and the crack opening displacements (CODs), which will form the intersection area in gas leakage path, as shown in Figure 1.

The present work focuses on the model based on Darcy's law. In this model, the crack density and the intersection area are required to compute the normalized permeability. There are a number of experimental and analytical works available in the literature investigating evolution of crack densities of transverse microcracking (see Ref. [17] and

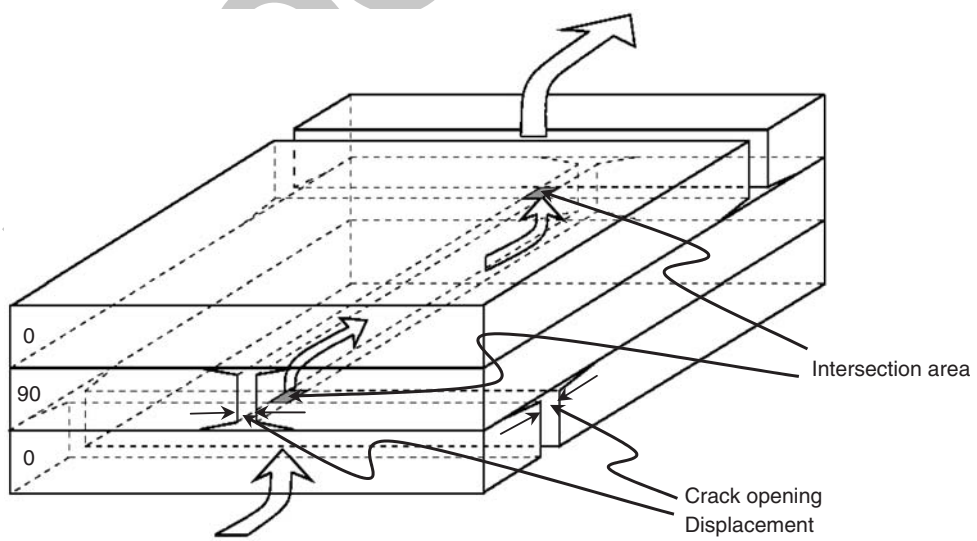

Figure 1. *Gas permeation pathway formed by microcracks and intersection areas in cross-ply laminates.*

references therein). Most of the analytical models, however, are 2-D models. Bapanapalli et al. [18] extended the 2-D model presented by Nairn [17], which is based on strain energy release rate concept, to a 3-D FEM-based model to predict crack densities in cross-ply laminate subjected to bi-axial loading. The intersection areas in cross-ply laminates were parametrically investigated in our previous work [15]. And it has been found that the local effect is significant and a 3-D finite element analysis is recommended to capture the details. In the current study, a prediction system based on FE modeling is set up, the progressive permeability in cross-ply laminate is predicted in terms of applied loads, and the material constant is quantified based on some experimental results available in the literature. All the finite element modeling are done using ABAQUS® standard FE package.

PERMEABILITY MODEL DESCRIPTION

The composite laminate with micro-cracks and delaminations is treated as a porous material. Hence, Darcy's Law for porous material is used:

$$q = -\frac{\kappa}{\mu}\nabla P \tag{1}$$

where q is the volume flow rate per unite area, k is the permeability tensor, m is the viscosity, and ∇P is pressure gradient vector. If we only consider the gas leak in the thickness direction of the laminate, the following one-dimensional form of Darcy's law can be used:

$$q = -\frac{k}{\mu}\frac{\partial P}{\partial z} \tag{2}$$

where k is the overall permeability in thickness direction and z is the thickness direction coordinate. The permeability k depends on the microstructure of the laminate. Integrating both side of Equation (2) over the laminate thickness gives:

$$qh = -\frac{k}{\mu}(P_N - P_0) \tag{3}$$

or:

$$-(P_N - P_0) = qh\frac{\mu}{k} \tag{4}$$

where h is the laminate thickness, and P_N and P_0 are pressure at the top and bottom respectively (Figure 2).

Also, if the integration is done layer-wisely, we have:

$$-(P_i - P_{i-1}) = qh_i\frac{\mu}{k_i}, \quad i = 1, \ldots, N \tag{5}$$

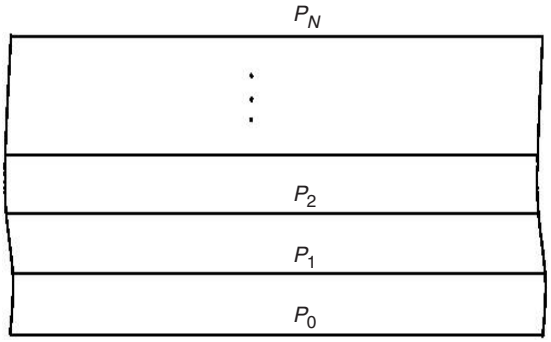

Figure 2. *Pressure distribution along thickness direction of laminate.*

where h_i and k_i are the thickness and permeability for each lamina. Summing Equation (5) from $i=1$ to $i=N$ yields:

$$-(P_N - P_0) = q\mu \sum_{i=1}^{N} \frac{h_i}{k_i}. \tag{6}$$

Comparing Equation (6) with Equation (4), it can be seen that:

$$\frac{h}{k} = \sum_{i=1}^{N} \frac{h_i}{k_i} \text{ or } k = \frac{h}{\sum_{i=1}^{N} h_i/k_i}. \tag{7}$$

For each lamina, most of the resistance comes from the intersection area. According to Poiseuille's Law, the volume flow rate in a rectangular tube (Figure 3) for the laminar flow is given by:

$$Q = \frac{d^4}{12\mu L} \Delta P. \tag{8}$$

Dividing both sides by the cross-section area of the tube, d^2, gives:

$$q = \frac{d^2}{12\mu} \frac{\Delta P}{L}. \tag{9}$$

Comparing Equation (9) with Equation (2), it can be seen that the permeability k for the rectangular tube is proportional to the cross-section area. Based on this fact, we can assume that the permeability for each lamina is proportional to the total intersection area. This assumption is also confirmed by Peddiraju et al. using FLUENT® simulation [10]. Noting that first and last laminas only have one interface with other laminas while others have two interfaces, the individual permeability is assumed to take the form:

$$\begin{aligned} k_1 &= C\lambda_1\lambda_2 A_{(1,2)} \\ k_i &= \frac{C\left(\lambda_{i-1}\lambda_i A_{(i-1,i)} + \lambda_i\lambda_{i+1} A_{(i,i+1)}\right)}{2}, \quad i = 2, \ldots, N-1 \\ k_N &= C\lambda_{N-1}\lambda_N A_{(N-1,N)} \end{aligned} \tag{10}$$

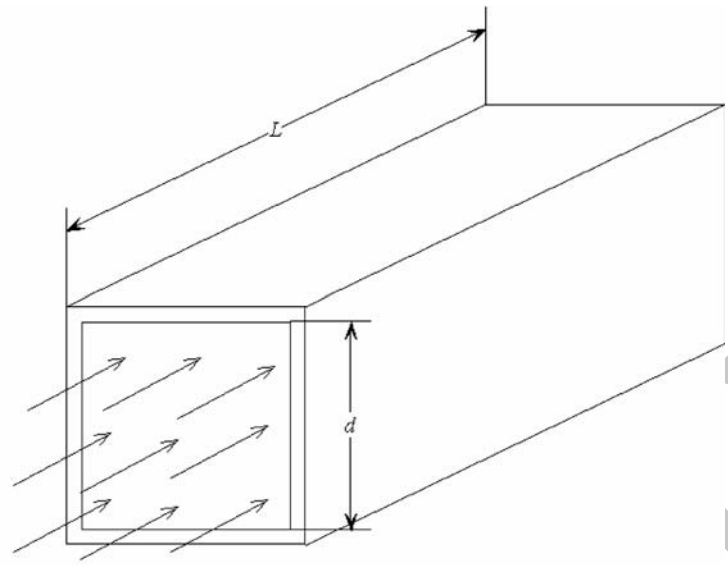

Figure 3. *Laminar flow in a rectangle tube.*

where λ_i is the crack density of the ith ply, $A_{(i,i+1)}$ is the individual intersection area between the ith and $i+1$th ply, and C is a material constant to be determined by experiments.

If we substitute k_i back into Equation (7), the overall permeability of laminate can be written as:

$$k = \frac{Ch}{h_1/\lambda_1\lambda_2 A_{(1,2)} + \sum_{i=2}^{N-1} h_i/\left(\lambda_{i-1}\lambda_i A_{(i-1,i)} + \lambda_i\lambda_{i+1}A_{(i,i+1)}\right) + h_N/\lambda_{N-1}\lambda_N A_{(N-1,N)}}. \quad (11)$$

Once the material property C is determined, the overall permeability k can be predicted by the crack densities and the intersection areas. Even though both the crack density and the intersection area are functions of force resultants N_x and N_y, fortunately, the following 2-D finite element analysis shows that these two factors can be decoupled, since crack density does not have much influence on the COD.

Figures 4(a) and (b) show the representative volume elements (RVEs) of two different scenarios that could occur in the composite laminate. The microcracks are usually generated in the 90°-ply and lead to the interfacial delamination between the 0°- and 90°-plies. Due to symmetry, one-fourth of the RVE is used for the 2-D finite element simulation. Eight-node isoparametric elements are used in the simulation and the orthotropic material properties used in the simulation are shown in Table 1. Figures 4(c) and (d) show the computed CODs with respect to the crack density. The CODs are expressed for unit force by normalizing with respect to the force resultant N_x, which is computed by volume average method. It can be seen that the CODs are almost constants for a given force resultant and delamination length.

From the above discussion, we can argue that the crack density does not influence the crack opening displacement. Hence the problem can be decoupled into two parts, first find

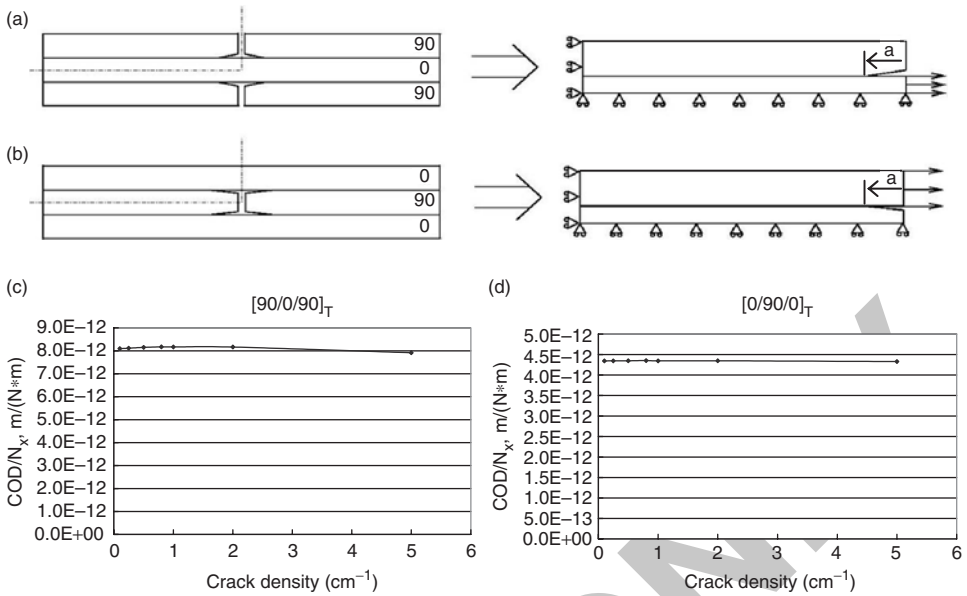

Figure 4. *Two-dimensional finite element model: (a) $[90/0/90]_T$, (b) $[0/90/0]_T$, and COD variation with respect to crack density: (c) $[90/0/90]_T$, (d) $[0/90/0]_T$*

Table 1. Orthotropic material properties for the composite.

Properties	E_1	E_2, E_3	G_{12}, G_{13}	G_{23}	ν_{12}, ν_{13}	ν_{23}
Value	169	8.62	5.0	1.22	0.355	0.410

the crack densities for a given load and then compute the intersection area. Then, the permeability for a given load can be computed using Equation (11).

METHODOLOGY

The crack densities and the intersection area are obtained using the following methods, and the progressive permeability is computed and plotted using a MATLAB program.

Crack Densities

The method developed by Bapanapalli et al. [18] is used to predict the crack density in each ply under bi-axial loading. The method is briefly reviewed in this section. Based on experimental observation [17], there are two kinds of scenarios when a cross-ply laminate is loaded in different direction under uniaxial loading, as shown in Figure 5. The microcracks in the middle ply and the surface ply are both evenly distributed.

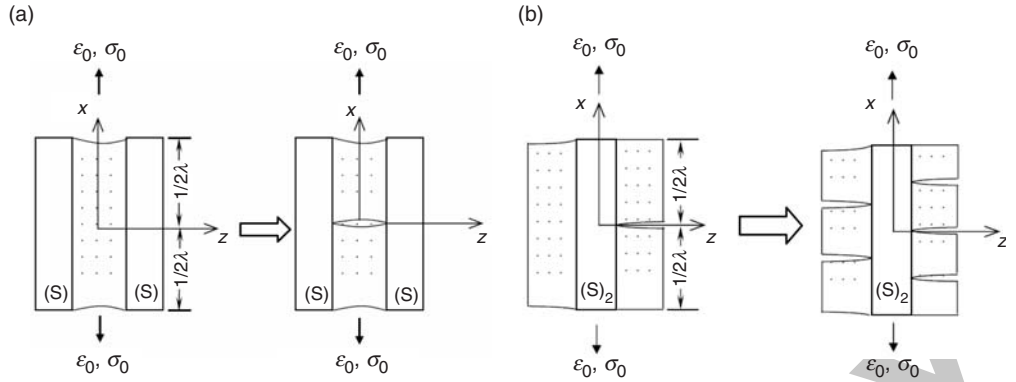

Figure 5. *Evolution of microcracks in the cross-ply laminate. (a) Cracks in the middle ply, (b) Cracks in the surface ply. [16]*

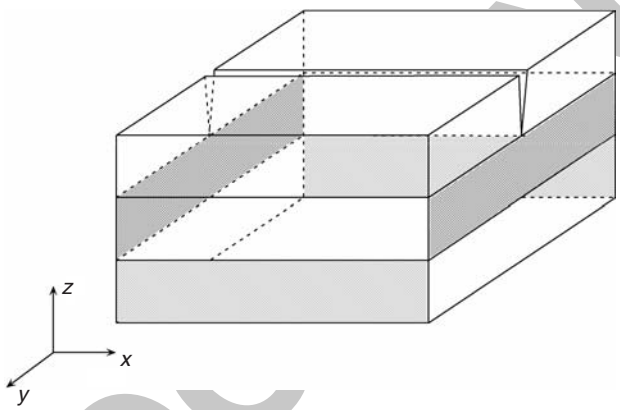

Figure 6. *Representative volume element with microcracks in both middle and surface plies (shaded areas are crack surfaces).*

Under bi-axial loading, microcracks can be generated in every ply of the cross-ply laminate. Hence, the RVE used in the current analysis is taken as shown in Figure 6. The applied loads in different directions are taken to be proportional to each other, i.e., $N_x/N_y = \alpha$. For example, in a cylindrical tank, $\alpha = 0.5$ or 2 and in a spherical tank, $\alpha = 1$.

There are three different cases that could happen for the next generated microcrack: case I, in the middle ply, case II, in the surface plies, and case III, in all plies. The strain energy released due to new crack formation is given by Equation (12), where $\Delta\overline{A}_{ij}$ are the differences of the inverse of the stiffness matrix before and after the formation of new cracks, and l_x and l_y are the crack spacing in the x- and y-directions. Equating this energy to the energies required for the three cases gives the required N_y, as shown in Equations (13) and (14), where G_{mc} is the microcracking fracture toughness and h_1 and h_2 are the surface ply thickness and the middle ply thickness respectively. Whichever case gives the lowest N_y would be the case that really happens. For the detailed derivation,

please refer to Ref. [18]. Using this method, the crack density will be predicted in terms of the applied load.

$$G_m = \frac{1}{2}\left(\alpha^2 \Delta\overline{A}_{11} + 2\alpha\Delta\overline{A}_{12} + \Delta\overline{A}_{22}\right) \times N_y^2 \times \frac{1}{l_x} \times \frac{1}{l_y} \tag{12}$$

$$N_{y(I)} = \sqrt{\frac{2G_{mc}h_2}{\left(\alpha^2 \Delta\overline{A}_{11} + 2\alpha\Delta\overline{A}_{12} + \Delta\overline{A}_{22}\right)1/\lambda_y}} \tag{13}$$

$$N_{y(II)} = \sqrt{\frac{8G_{mc}h_1}{\left(\alpha^2 \Delta\overline{A}_{11} + 2\alpha\Delta\overline{A}_{12} + \Delta\overline{A}_{22}\right)1/\lambda_x}} \tag{14}$$

$$N_{y(III)} = \sqrt{\frac{2\left[(G_{mc}(1/\lambda_x)h_2) + \left(4G_{mc}(1/\lambda_y)h_1\right)\right]}{\left(\alpha^2 \Delta\overline{A}_{11} + 2\alpha\Delta\overline{A}_{12} + \Delta\overline{A}_{22}\right)1/\lambda_x(1/\lambda_y)}}. \tag{15}$$

Intersection Areas

Once the crack densities are determined, the dimension of the RVE is fixed. Because of the symmetry, only one-quarter of the RVE is taken in the model, as shown in Figure 7(a). The shaded surfaces are the microcrack surfaces. Delaminations are introduced in this model since no intersection area will be formed without delamination. The effect of the delamination length on the intersection area was investigated in our previous work [15]. In the current work, a fixed delamination length is taken and most attention will be paid to investigating the variation of permeability with respect to the applied loads. It has been shown in our previous work [15] that the local effect of geometry on the CODs at the cross-section is significant and a 3-D FEM model is necessary to accurately obtain the intersection areas. And since the problem is decoupled, a typical crack density is taken, $\lambda_x = \lambda_y = 2.0/\text{cm}$, to do the simulation. The ply thickness is taken as 0.33 mm. Figure 7(b) shows a typical deformation of the lay-up $[0/90/0]_T$ under bi-axial loading. Note that the deformation is enlarged by a factor of 10.

RESULTS AND DISCUSSION

Three lay-ups are investigated: $[0/90/0]_T$, $[0/90_2/0]_T$, and $[0/90_4/0]_T$. First, the damage evolution in these laminates under uniaxial loading is investigated to validate the method. From experimental observation [17,19], it has been found that the initial stress for microcracks in the middle ply is less for thicker middle ply and the initial stress for microcracks in surface ply is greater for thicker middle ply. However, at high stress levels, greater crack density was observed in the thinner middle ply. Figure 8 shows the crack densities in different laminates predicted using the aforementioned method under uniaxial loading. A typical value of microcracking fracture toughness G_{mc} is taken as 240 J/m [17]. In Figure 8(a), the stress to initiate first microcrack increases as the middle ply thickness decreases. But, once the initiation stress is reached, the crack density increases faster in the laminate with thinner middle ply. For $[0/90/0]_T$, even a negative slope is obtained, which means that the microcracks accumulate simultaneously in the laminate. In Figure 8(b),

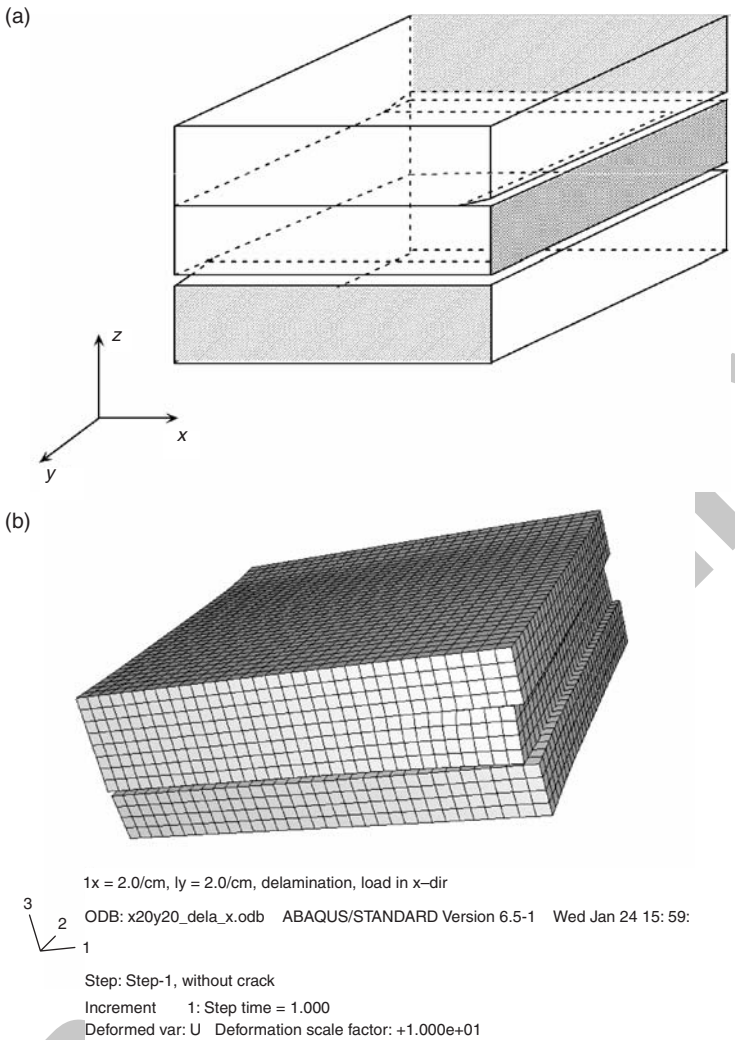

Figure 7. *Three-dimensional delamination model and typical deformation.*

as the middle ply thickness of laminate increases, the initiation stress increases as well. Hence, our prediction and experimental observation match quite well qualitatively.

In reality, the laminate used in the propellant tank is under bi-axial loading. The proportional constant α between force resultants N_x and N_y is taken as 0.5, 1.0 and 2.0 to represent different possible stress states in the hydrogen tank. Figure 9 shows the variations of crack densities in different laminates under different biaxial loading. For each laminate, crack densities λ_x and λ_y are plotted in same figure with respect to the average stress in the y-direction (N_y divided by the laminate thickness). Figures 9(a)–(c) represent the cases when $\alpha = 0.5$, (d)–(f) represent $\alpha = 1.0$, and (g)–(i) represent $\alpha = 2.0$. From these figures, it can be seen that the initiation stresses for first microcrack in both x- and y-directions are lower than their corresponding values under uniaxial loading. With the

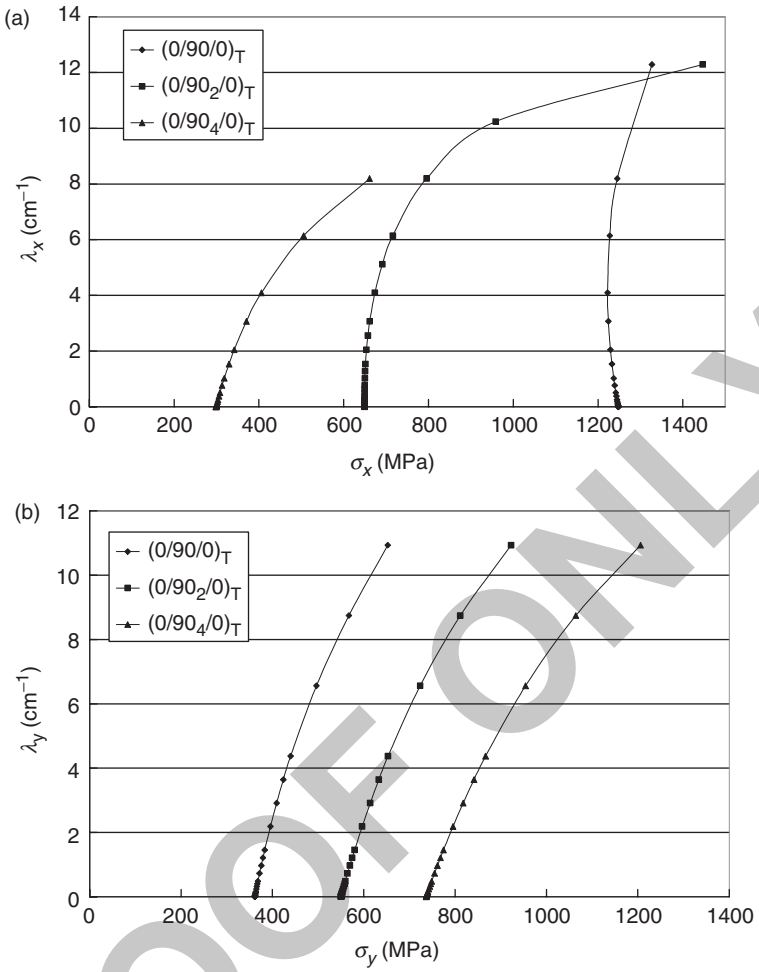

Figure 8. *Damage evolution under uniaxial loading. (a) Load in x-direction and microcracks in middle ply, (b) Load in y-direction and microcracks in surface ply.*

same proportional constant α, the initial stress for λ_x decreases dramatically as the middle ply thickness increase. On the contrary, the initial stress for λ_y increases as the middle ply thickness increases, but the increasing rate is not as great as that under uniaxial loading. Loads in the x-direction affect the crack densities in the y-direction. For the same laminate, say $[0/90/0]_T$, when α increases (σ_x increases), the initiation stress for λ_y decreases. No microcracks are generated in $[0/90/0]_T$ for $\alpha = 0.5$ and 1.0 when λ_y already meet the preset stress limit.

After all the crack densities are predicted, the intersection areas need to be computed. Table 2 shows the intersection area of two typical cases (case I: $\varepsilon_x = 1\%$, $\varepsilon_y = 0$, case II: $\varepsilon_x = 0$, $\varepsilon_y = 1\%$) for different lay-ups obtained using the aforementioned delamination model. These typical values are the basis to compute the areas at particular loads, see Ref. [15] for details. From this table, it can be seen that the intersection areas increase as the thickness of the middle ply increases.

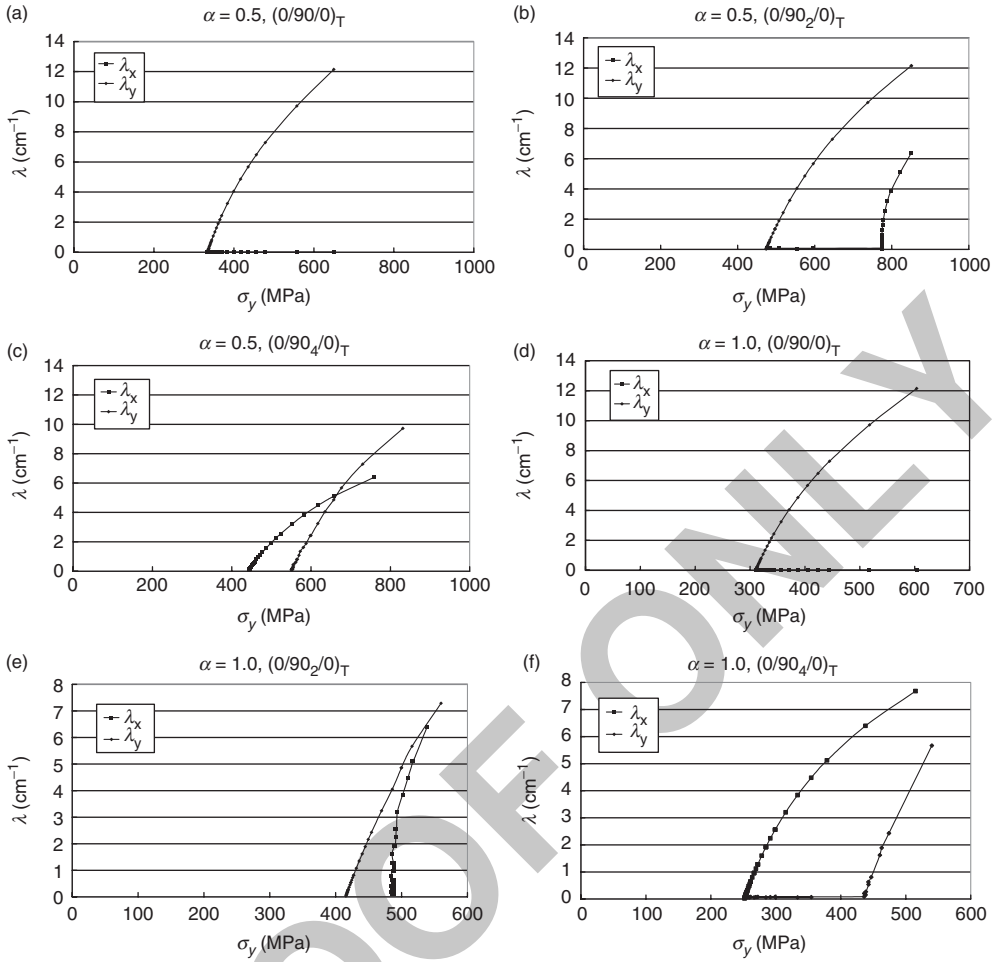

Figure 9. *Damage evolution under biaxial loading. (a)–(c), $\sigma_x/\sigma_y = 0.5$, (d)–(f), $\sigma_x/\sigma_y = 1.0$, (g)–(i), $\sigma_x/\sigma_y = 2.0$.*

Table 2. Intersection areas of cracks for different laminates under two typical load cases.

Lay-ups	Case I: $\varepsilon_x = 1\%$, $\varepsilon_y = 0$	Case II: $\varepsilon_x = 0$, $\varepsilon_y = 1\%$
$[0/90/0]_T$	0.8316×10^{-10}	0.7725×10^{-10}
$[0/90_2/0]_T$	1.0545×10^{-10}	1.0072×10^{-10}
$[0/90_4/0]_T$	1.2549×10^{-10}	1.1803×10^{-10}

Substituting the crack densities and the intersection areas into Equation (11), the progressive permeability in composite laminates can be predicted as shown in Figures 10–12. Since the material constant C needs to be determined from experiments, the permeability is normalized by the constant C.

In order to form a contiguous gas leakage pathway microcracks have to be developed in every ply. In Figures 10 and 11, no permeations are predicted for laminate $[0/90/0]_T$

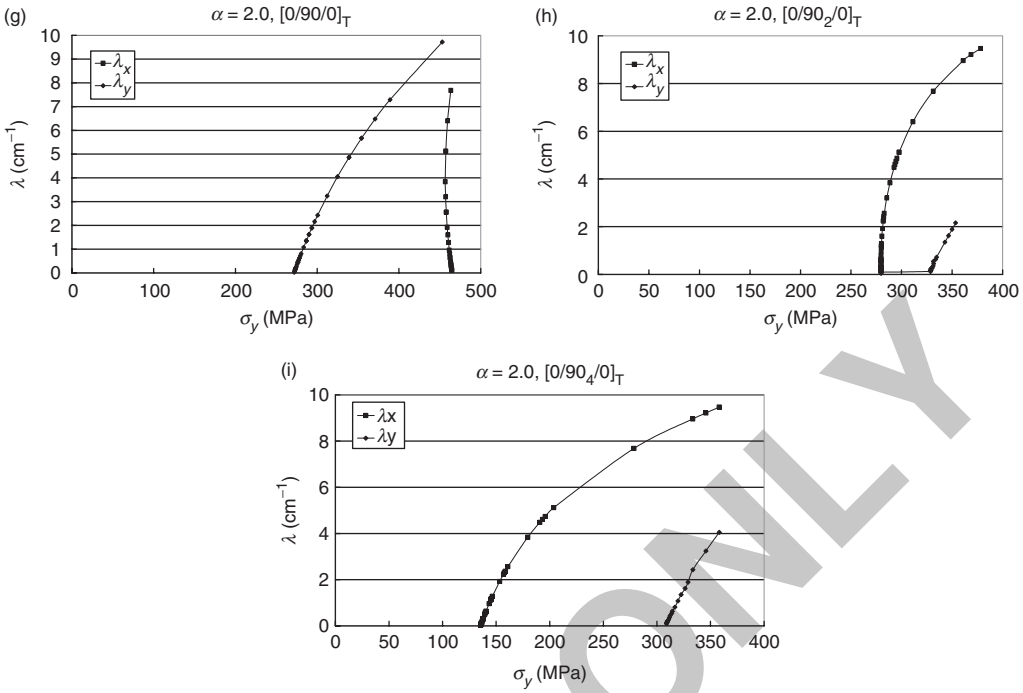

Figure 9. *Continued.*

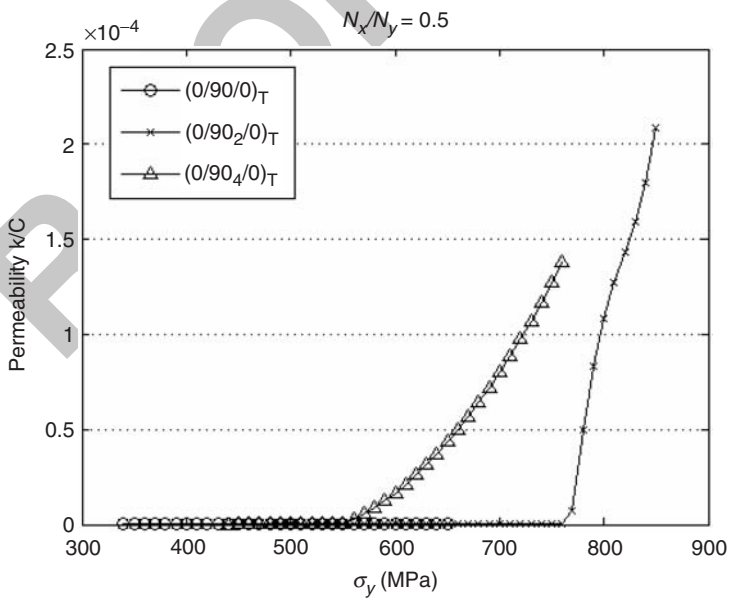

Figure 10. *Predicted permeability in laminates for $N_x/N_y = 0.5$.*

3

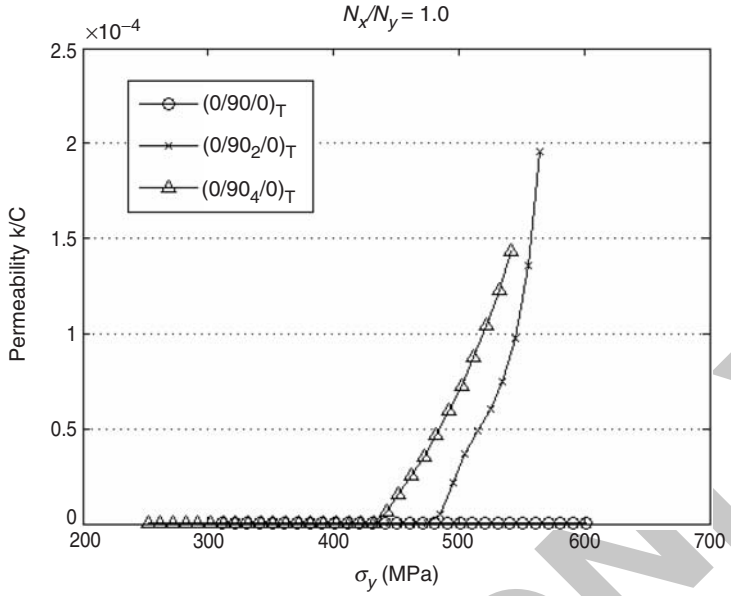

Figure 11. *Predicted permeability in laminates for $N_x/N_y = 1.0$.*

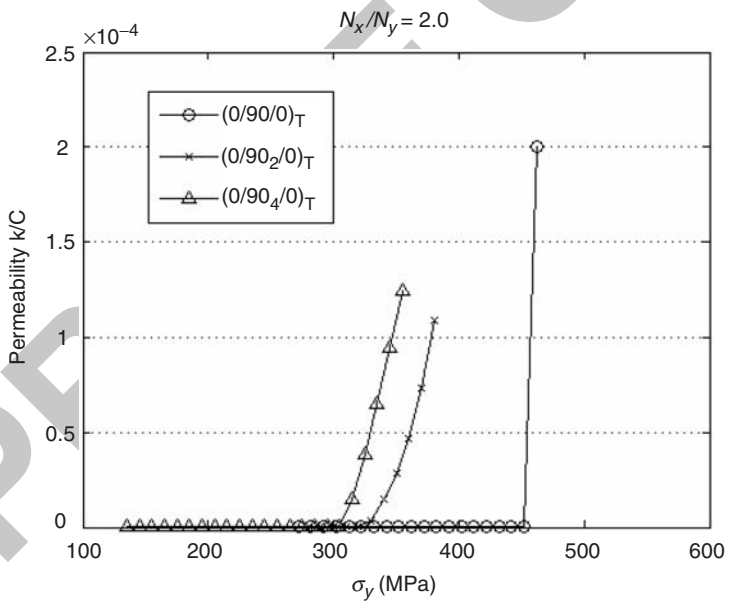

Figure 12. *Predicted permeability in laminates for $N_x/N_y = 2.0$.*

4

since no microcrack is predicted in the middle ply under given stress level (Figure 9(a) and (d)). But once the permeation is predicted in $[0/90/0]_T$ (Figure 13), it increases very quickly because the microcracks accumulate simultaneously. For laminates $[0/90_2/0]_T$ and $[0/90_4/0]_T$, the initiation stress for permeation is affected by the proportional constant α.

Figure 13. ▮▮▮▮.

Table 3. Experimental data and computed constant C.

Lay-up	λ_0 (cm^{-1})	λ_{90} (cm^{-1})	Measured permeability (m^3/m^2/s)	Material constant C(m^3/m^2/s)
$[0/0/90/90]_s$	1.0	7.0	1.3e-7	0.00378
$[0/90/0/90]_s$	1.4	7.0	2.8e-8	0.00232

For both laminates, initiation stresses decrease as α increases, but the influence on $[0/90_2/0]_T$ is more significant. For all α, the initiation stress for $[0/90_2/0]_T$ is greater than the one for $[0/90_4/0]_T$. Once it starts to permeate, the permeability in $[0/90_2/0]_T$ increases faster than in $[0/90_4/0]_T$ even though the intersection areas in $[0/90_4/0]_T$ are bigger, which shows that the crack densities play a more important role in the permeability.

From the predicted permeability variation, it can be seen that thinner middle ply leads to higher initiation stress. But, once it starts to permeate, the thinner middle ply causes rapid increase in permeation.

QUANTIFICATION OF CONSTANT C

Kumazawa et al. [3, 4] have performed experimental work on damage and permeability in cross-ply laminates. In this section, we try to quantify the material constant C based on their experimental data. Two different cross-ply laminates with lay-ups $[0/0/90/90]_s$ and $[0/90/0/90]_s$ were tested by Kumazawa et al. The crack densities in the 0°- and 90°-plies and the permeability were measured as a function of applied strain. In this work, we take two sets of values from their experiments and quantify the constant C. The crack densities, the measured permeability, and computed constant C are listed in Table 3. The permeability was measured under strain $\varepsilon_x = \varepsilon_y = 0.1\%$ and the curing temperature of the composite is 180°C. Hence, in our model, the RVE is loaded at $\varepsilon_x = \varepsilon_y = 0.1\%$ and $\Delta T = -160$°C. The material properties in Table 1 are still used.

From Table 3, it can be seen that the computed material constant C for both laminates are in the same order of magnitude. They are not exactly the same because the modeling results are influenced by other factors such as delamination length and delamination shape [15]. Hence, more detailed experimental data are needed in order to accurately quantify the constant C. However, based on the limited experimental data in conjunction with our analysis we are able to obtain a range for the constant C as shown in Table 3.

CONCLUSIONS

In the present work, a permeation model based on Darcy's law is used to predict the gas permeability in cross-ply laminate under bi-axial loading. The problem is decoupled into two steps: prediction of crack density and computing intersection area. Three-dimensional finite element analysis is used in both steps. The variations of permeability as a function of average stress for three cross-ply laminates with different lay-ups ($[0/90/0]_T$, $[0/90_2/0]_T$, and $[0/90_4/0]_T$) are investigated. From the prediction, it can be seen that $[0/90/0]_T$ laminates require the highest stress for initiation of leakage, but once it starts to leak the permeability increases very fast. It also can be seen that the crack density has more influence on permeability than the intersection area. Hence it is suggested that the design of laminates should try to avoid thicker ply groups. Finally, the material constant involved in the permeability prediction is quantified based on experimental data available in the literature.

ACKNOWLEDGMENTS

This work is supported by NASA Glenn Research Center (NAG3-2750) and NASA Kennedy Space Center under the Hydrogen Research and Education Program. The authors gratefully thank their technical and financial support.

REFERENCES

1. Kessler, S.S., Matuszeski, T. and McManus, H. (2001). Cryocycling and Mechanical Testing of CFRP for the X-33 Liquid H_2 Fuel Tank Structure, In: *Proceedings of the 16*th *Annual Technical Conference of the American Society for Composites (ASC)*, ASC-2001-093, Blacksburg, VA, Sept. 9–12.
2. Kumazawa, H., Aoki, T. and Susuki, I. (2003). Analysis and Experiment of Gas Leakage through Composite Laminates for Propellant Tanks, *AIAA Journal*, **41**(10): 2037–2044.
3. Kumazawa, H., Susuki, I. and Aoki, T. (2006). Gas Leakage Evaluation of CFRP Cross-ply Laminates under Biaxial Loadings, *Journal of Composite Materials*, **40**(10): 853–871.
4. Kumazawa, H., Hayashi, H., Susuki, I. and Utsunomiya, T. (2006). Damage and Permeability Evolution in CFRP Cross-Ply Laminates, *Composite Structures*, **76**: 73–81.
5. Aoki, T., Kumazawa, H. and Susuki, I. (2002). Propellant Leakage through Laminated Structures, In: *Proceedings of the 17th Annual Technical Conference of the American Society for Composites (ASC)*, pp. 63–70, West Lafayette, IN.
6. Peddiraju, P., Grenoble, R., Fried, K., Gates, T. and Lagoudas, D.C. (2005). Analytical Predictions and Experimental Measurements of Hydrogen Permeability in a Microcrack Damaged Composites, In: *Proceeding of 46th AIAA/ASME/ASCE/AHS/ASC Structures, Structural Dynamics and Materials Conference*, pp. 18–21, AIAA 2005-2087, Austin, TX.

7. Grenoble, R.W. and Gates, T.S. (2005). Hydrogen Permeability of Polymer Matrix Composites at Cryogenic Temperatures, In: *Proceeding of 46th AIAA/ASME/ASCE/AHS/ASC Structures, Structural Dynamics and Materials Conference*, pp. 18–21, AIAA 2005-2086, Austin, TX.
8. Bechel, V.T. and Arnold, F. (2006). Permeability of Polymer Composites for Cryogenic Applications, In: *Proceeding of 47th AIAA/ASME/ASCE/AHS/ASC Structures, Structural Dynamics and Materials Conference*, pp. 1–4, AIAA 2006-2015, Newport, RI.
9. Choi, S., Sankar, B.V. Gas Permeability of Various Graphite/Epoxy Composite Laminates for Cryogenic Storage Systems, *Composites Part B: Engineering* (in press).
10. Peddiraju, P., Noh, J., Whitcomb, J. and Lagoudas, D.C. (2007). Prediction of Cryogen Leak Rate through Damaged Composite Laminates, *Journal of Composite Materials*, **41**(1): 41–71.
11. Noh, J., Whitcomb, J., Peddiraju, P. and Lagoudas, D. (2004). Prediction of Leakage Rate through Damage Network in Cryogenic Composite Laminates, In: *Proceeding of 45th AIAA/ASME/ASCE/AHS/ASC Structures, Structural Dynamics and Materials Conference*, pp. 19–22, AIAA 2004-1861, Palm Springs, CA.
12. Peddiraju, P., Lagoudas, D., Noh, J. and Whitcomb, J. (2004). Numerical Modeling of Cryogen Leakage through Composite Laminates, In: *Proceeding of 45th AIAA/ASME/ASCE/AHS/ASC Structures, Structural Dynamics and Materials Conference*, pp. 19–22, AIAA 2004-1862, Palm Springs, CA.
13. Roy, S. and Benjamin, M. (2004). Modeling of Permeation and Damage in Graphite-epoxy Laminates for Cryogenic Fuel Storage, *Composites Science and Technology*, **64**: 2051–2065.
14. Roy, S. and Nair, A. (2006). Modeling of Permeability in Composite Laminates with Delaminations and Stitch Cracks, In: *Proceeding of 47th AIAA/ASME/ASCE/AHS/ASC Structures, Structural Dynamics and Materials Conference*, AIAA-2006-2094, May 1–4, Newport, RI.
15. Xu, J.L. and Sankar, B.V. (2007). Parametric Investigation of Gas Permeability in Cross-ply Laminates using Finite Elements, *AIAA Journal*, **45**(4): 934–941.
16. McManus, H.L., Faust, A. and Uebelhart, S. (2001). Gas Permeability of Thermally Cycled Graphite-epoxy Composites, *American Society for Composites*, Blacksburg, VA, Paper 092, Sept. 9–12.
17. Nairn, J.A. (2000). Matrix Microcracking in Composites, in *Polymer Matrix Composites*, Edited by Talreja, R. and Manson, J-A. Volume 2 of *Comprehensive Composite Materials*, Elsevier Science, Chapter 13.
18. Bapanapalli, S.K., Sankar, B.V. and Primas, R.J. (2006). Microcracking in Cross-ply Laminates due to Biaxial Mechanical and Thermal Loading, *AIAA Journal*, **44**(12): 2949–2957.
19. Nairn, J.A., Hu, S.F. and Bark, J.S. (1993). A Critical Evaluation of Theories for Predicting Microcracking in Composite Laminates, *Journal of Materials Science*, **28**: 5099–5111.